Homogenized Variability of Radiosonde-Derived Atmospheric Boundary Layer Height over the Global Land Surface from 1973 to 2014

XIAOYAN WANG

College of Global Change and Earth System Science, Beijing Normal University, and Joint Center for Global Change Studies, Beijing, China, and Department of Geological Sciences, Jackson School of Geosciences, The University of Texas at Austin, Austin, Texas

KAICUN WANG

College of Global Change and Earth System Science, Beijing Normal University, and Joint Center for Global Change Studies, Beijing, China

(Manuscript received 28 October 2015, in final form 3 July 2016)

ABSTRACT

Boundary layer height (BLH) significantly impacts near-surface air quality, and its determination is important for climate change studies. Integrated Global Radiosonde Archive data from 1973 to 2014 were used to estimate the long-term variability of the BLH based on profiles of potential temperature, relative humidity, and atmospheric refractivity. However, this study found that there was an obvious inhomogeneity in the radiosonde-derived BLH time series because of the presence of discontinuities in the raw radiosonde dataset. The penalized maximal F test and quantile-matching adjustment were used to detect the changepoints and to adjust the raw BLH series. The most significant inhomogeneity of the BLH time series was found over the United States from 1986 to 1992, which was mainly due to progress made in sonde models and processing procedures. The homogenization did not obviously change the magnitude of the daytime convective BLH (CBLH) tendency, but it improved the statistical significance of its linear trend. The trend of nighttime stable BLH (SBLH) is more dependent on the homogenization because the magnitude of SBLH is small, and SBLH is sensitive to the observational biases. The global daytime CBLH increased by about 1.6% decade^{-1} before and after homogenization from 1973 to 2014, and the nighttime homogenized SBLH decreased by −4.2% decade^{-1} compared to a decrease of −7.1% decade^{-1} based on the raw series. Regionally, the daytime CBLH increased by 2.8%, 0.9%, 1.6%, and 2.7% decade^{-1} and the nighttime SBLH decreased significantly by −2.7%, −6.9%, −7.7%, and −3.5% decade^{-1} over Europe, the United States, Japan, and Australia, respectively.

1. Introduction

The atmospheric boundary layer is the lowest layer of the troposphere that is directly influenced by Earth's surface (Seibert et al. 2000). Substances emitted into this layer disperse gradually, both horizontally and vertically through turbulence, and become completely mixed within a time scale of approximately one hour (Eresmaa et al. 2006; Seibert et al. 2000). Processes within the boundary layer control the exchanges of momentum, heat, water, and trace substances (i.e., aerosols) between Earth's surface and the atmosphere (Garratt 1993; Schmid and Niyogi 2012; Seibert et al. 2000). It is important to determine the boundary layer height (BLH) to facilitate an understanding of the transport process in the troposphere, and for effective weather prediction and climate monitoring (Garratt 1993; Lee and Kawai 2011). The BLH is a key parameter in air pollution models

Denotes Open Access content.

Supplemental information related to this paper is available at the Journals Online website: http://dx.doi.org/10.1175/JCLI-D-15-0766.s1.

Corresponding author address: Dr. Kaicun Wang, College of Global Change and Earth System Science, Beijing Normal University, No. 19 Xinjiekouwai Street, Beijing 100875, China.
E-mail: kcwang@bnu.edu.cn

Publisher's Note: This article was revised on 19 September 2016 to correct an error in the last sentence of the first paragraph on p. 6896 (section 2b).

DOI: 10.1175/JCLI-D-15-0766.1

because it determines the volume available for pollutants to disperse into (Eresmaa et al. 2006; Gupta et al. 1997; Hong and Pan 1998; Jordan et al. 2010; Lee and Kawai 2011; Liu and Liang 2010; Seibert et al. 2000; Zhang et al. 2011). Long-term variation in the BLH can drive changes in air quality, and its determination is important in climate change studies (Yang et al. 2013; Zhang et al. 2013).

However, our knowledge of the global BLH is very limited. Climatological analyses of the BLH have been undertaken over some areas (Fetzer et al. 2004; Gryning and Batchvarova 2002; Johansson et al. 2001; Ratnam et al. 2010; Sempreviva and Gryning 2000), but very few attempts have been made to estimate a global and long-term BLH. Existing studies of the BLH are highly localized, and the data have been obtained over relatively short time periods (Chan and Wood 2013; Hennemuth and Lammert 2006; Seidel et al. 2010; White et al. 1999; Zhang et al. 2013). The available long-term global radiosonde dataset is the most common data source for the operational determination of the BLH (Seibert et al. 2000), and the BLH derived from radiosonde data has been widely used as the reference to evaluate the estimates obtained using other datasets or model simulations (Dai et al. 2011; Eresmaa et al. 2006; Ferrero et al. 2011; Lee and Kawai 2011; Lewis et al. 2013; von Engeln and Teixeira 2013).

The raw radiosonde data records have been shown to contain many spurious changes and discontinuities resulting from changes in instruments, observational practices, processing procedures, station relocations, and other issues (Dai et al. 2011; Elliott and Gaffen 1991; Elliott et al. 1998; Haimberger 2007; Parker and Cox 1995; Zhao et al. 2012). Numerous methods have been proposed to homogenize the raw radiosonde dataset at mandatory pressure levels (i.e., temperature, humidity, and wind profiles) (Haimberger et al. 2012; McCarthy et al. 2009, 2008; Pattantyús-Ábrahám and Steinbrecht 2015; Sherwood et al. 2008; Thorne et al. 2011; Titchner et al. 2009; Zhai and Eskridge 1996); however, there has not been a study that has focused on the homogenization of the radiosonde-derived variables such as BLH, which was estimated based on the original radiosonde vertical resolution rather than on the mandatory pressure levels.

In this study, we found significant inhomogeneity issues that were relevant to the radiosonde-derived BLH time series, particularly in the United States (see section 2c for detailed information). Therefore, we attempted to homogenize the radiosonde-derived BLH; that is, we used statistical changepoint detection and adjustment methods to homogenize the BLH time series derived from the Integrated Global Radiosonde Archive (IGRA) released by the National Climatic Data Center (NCDC). This paper is the first attempt to homogenize BLH derived from radiosonde data over the global land surface from 1973 to 2014, and the long-term variabilities of convective BLH (CBLH) and stable BLH (SBLH) based on the raw data and homogenized time series are reported. These results have important implications for climate change, especially for the long-term variability of air quality and land–atmosphere energy and mass exchanges.

2. Data and methodology

a. Dataset

Radiosonde data are available on a global scale. The data quality is well controlled by the NCDC IGRA project (Durre et al. 2006, 2008), which provides the most commonly used data source for the operational determination of the BLH (Garratt 1994; Seibert et al. 2000). The latest version of the NCDC IGRA consists of a historical dataset from 1110 globally distributed stations, with quality-assured daily radiosonde records, and includes observed temperature, geopotential height, humidity, and derived variables (e.g., potential temperature and atmospheric refractive index) at mandatory pressure levels, additionally required levels, and thermodynamically significant levels (Durre and Yin 2008; Durre et al. 2006; Sorbjan 1989). The vertical resolution and extent of the soundings have improved significantly over time, with approximately three-quarters of all soundings extending to at least 100 hPa by 2003 (Durre et al. 2006).

b. The method used to estimate BLH

In this study, both the CBLH and SBLH were examined. For the stable boundary layer (SBL), the top of the surface-based inversion was defined as the SBLH. As shown in Fig. 1a, because air temperature increased with the increase of altitude below 253 m, the BLH was estimated to be 253 m. If no surface-based inversion occurred in the sounding profile, we considered it to be a convective or neutral boundary layer.

The convective boundary layer (CBL) can be identified as a transition from a convectively less stable region below to a more stable region above (Garratt 1994; Sorbjan 1989) and is a moister, more refractive region than the overlying troposphere. Thus, the CBLH can typically be defined as the level of the breakpoint of a temperature or humidity variable profile. Many methods have been proposed to estimate the CBLH based on an individual atmospheric variable relevant to the topic being investigated (Seibert et al. 2000; Wang and Wang 2014; Zhang et al. 2010).

The existing methods generally identify the level of the maximum vertical gradient of potential temperature θ, or the minimum gradient of relative humidity (RH) or refractivity N as the top of the boundary layer. In some cases, the BLH values derived from these three methods

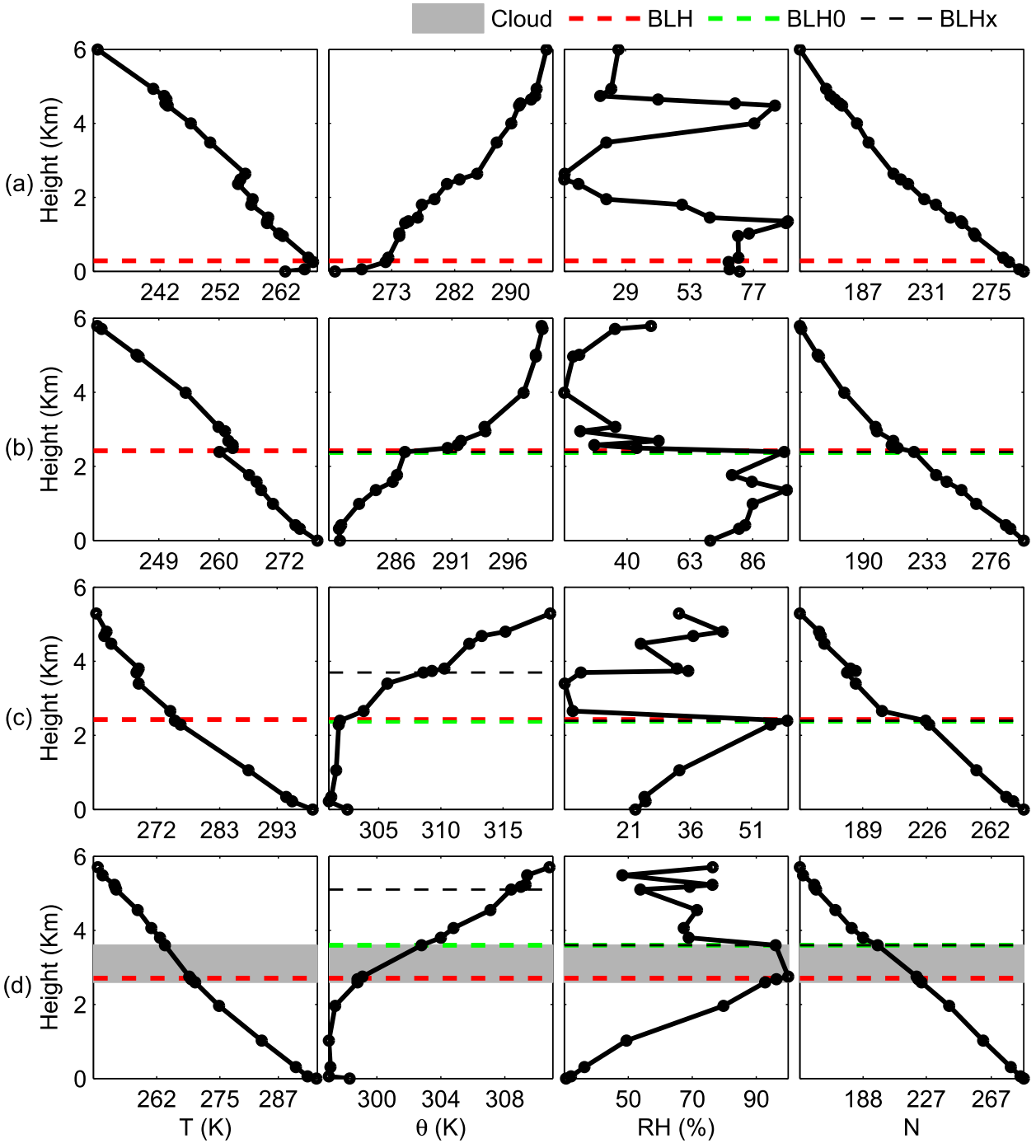

FIG. 1. Profiles of T, θ, RH, N, and the derived BLH. BLH_x indicates the boundary layer height derived from the individual variables (θ, RH, and N). BLH_0 indicates the height that best meets all of the variables. BLH is the final boundary layer height, integrating the information about θ, RH, N, and clouds. Gray shading indicates the locations of clouds. All four cases were obtained from Canadian station 71203 (49.95°N, 119.4°W): (a) stable boundary layer at 0424 LST 6 Feb 2001, (b) three individual methods consistent at 1624 LST 10 Feb 2010, (c) three methods inconsistent under clear-sky conditions at 1624 LST 22 Aug 1999, and (d) boundary layer cloud conditions at 1624 LST 23 Jul 2011.

are in good agreement, as shown in Fig. 1b. However, the difference in the BLH between the different methods could be as large as a few hundred meters, especially for an imperfectly mixed boundary layer, as shown in Fig. 1c, where the profiles of RH and atmospheric N defined the CBLH as 2397m above ground level (AGL), which was quite different from that derived from the potential temperature (3698m AGL).

Our previous study analyzed the reasons for these inconsistencies (i.e., the inconsistencies in the temperature and humidity profiles, the changing measurability of the atmospheric N with height, the measurement error of humidity instruments within clouds, and the presence of clouds; Wang and Wang 2014). A method that is able to integrate information about temperature, humidity, and clouds was proposed to estimate a consistent CBLH and was applied to radiosonde data in the United States (Wang and Wang 2014). This method was applied to the IGRA dataset in this study and is briefly introduced below.

1) Diagnose the effectiveness of the daily sounding profile

Given the change of station altitude because of station relocation, the height of the first level in each sounding was taken as the ground level. To guarantee an adequate vertical resolution, the soundings were accepted only if there were at least 10 levels below 5000 m AGL. To avoid mistaking free tropospheric features for the top of the boundary layer, we restricted the available data of all the sounding records to 5000 m AGL.

2) Identify the height that best satisfies the θ, RH, and N criteria as the interim boundary layer height (BLH_0)

The levels of the first three minimum (or maximum for θ) gradients of each variable profile were considered to satisfy the criterion of the top of the convective boundary layer and were likely to be the BLH. We identified the lowest level where at least two of the three variables met the requirement of the top of the boundary layer as the BLH_0, which indicated that all three of these variables exhibited a sharp variation at the level of BLH_0, but might be not the sharpest transitions in the entire profile. The allowable error was 100 m. If no consistent altitude was noted in any of the first three gradient levels, then the BLH_0 for this record was considered to be missing, and the following steps were not performed.

3) Derive the location of the boundary layer cloud

The top of the boundary layer cloud is typically defined as the top of the convective boundary layer, because of its sharp decrease in RH. However, the deep stable stratification in the cloud will suppress the development of turbulence, in which case the convective BLH should be located at the base of the stable layer.

We derived the location of the cloud based on the validated method proposed by Zhang et al. (2010).

1) Transform the RH profiles with respect to ice rather than liquid water, for all levels with temperatures below 0°C.
2) Derive the boundary of the moist layer where the observed RH exceeded the minimum-RH threshold for that level, as listed in Table S1 in the supplemental material.
3) Define the moist layer as a cloud layer if the maximum RH of the moist layer exceeded the corresponding maximum RH (Table S1 in the supplemental material) at the base of the moist layer.

4) Determine the final consistent BLH

If the BLH_0 was lower than the base of the lowest cloud or was identified as clear-sky conditions, then the BLH_0 was the final BLH. As shown in Fig. 1c, no cloud was formed based on the RH profile. Thus, the BLH_0 overlapped with BLH.

If the convective BLH_0 was higher than the base of the lowest cloud, and there was also a stable stratification deeper than 200 m in this boundary layer cloud, then the base of the stable layer was defined as the BLH (Fig. 1d). The bulk Richardson method has been shown to be suitable for both the stable and convective boundary layers (Glickman 2000; Vogelezang and Holtslag 1996; Zhang et al. 2013; Zilitinkevich and Baklanov 2002), in which both the temperature and wind field are considered. However, we found that at most of the IGRA stations wind speed and wind direction information were only available at some mandatory levels, which made it difficult to make full use of all the available radiosonde data. Thus, only the potential temperature, RH, and N profiles were used to define BLH.

To reduce the impact of the missing data, we calculated the monthly BLH only if the daily BLH values were available for more than 15 days in a month, and the annual BLH was calculated only if monthly values were available for more than six months in a year. Figure 2 shows the time series of the number of available stations. The number of IGRA stations increased sharply in 1964. However, the number of stations with effective annual BLH significantly increased in 1973 and remained stable afterward. Therefore, we limited our analysis to the period from 1973 to 2014. A total of 846 stations with more than 10 years of effective data were included in this study.

c. *Method to homogenize the BLH series*

We checked the BLH time series for each station and found clear discontinuities in some monthly BLH series

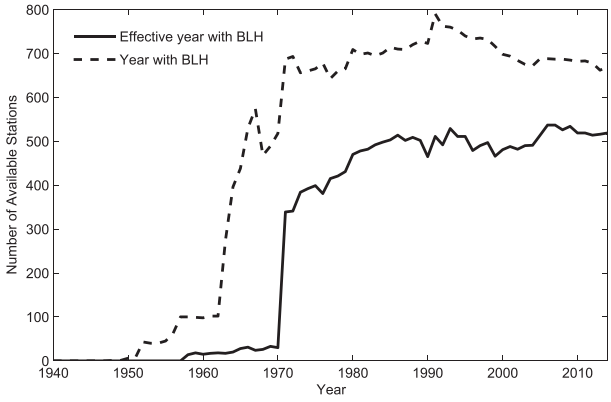

FIG. 2. Time series of the number of available stations in the IGRA dataset. Monthly BLH data were calculated only if the daily values were available for more than 15 days during a month, and the annual BLH was calculated only if monthly values were available for more than six months in a year. The dashed line indicates the number of stations with effective daily BLH data, and the solid line is the number of stations with an effective annual BLH. The number of IGRA stations increased sharply in 1964, and the number of stations with an effective annual BLH increased since 1973.

(as shown in Fig. 3). Figure 3 shows the BLH time series at a U.S. station (station 72451) before and after homogenization. During the period from September 1989 to December 1992, there was a significant discontinuity of BLH series at this station, with a sharp increase in the occurrence of SBLH. Therefore, homogenization tests had to be performed on the BLH time series. Most of the existing homogenization methods use neighboring station data as the reference series. However, radiosonde stations are very sparsely distributed, and it is difficult to identify an effective neighboring station. In addition, the sounding systems were generally replaced or upgraded throughout a country at approximately the same time, and therefore the neighboring station may suffer from the same inhomogeneity problem.

In this study, we used the publicly available software RHtestsV4 (http://etccdi.pacificclimate.org/software.shtml), which has been widely used (Venema et al. 2012), to detect breakpoints in monthly radiosonde-derived BLH data, and to make necessary adjustments. RHtestsV4 detects and adjusts changepoints in data series that may have first-order autoregressive errors (Wang and Feng 2013). It includes two algorithms to detect changepoints: the PMTred algorithm, which is based on the penalized maximal t test (PMT), and the PMFred algorithm, which is based on the penalized maximal F test (PMF). The PMT works with a reference series, and the PMF can be made without a reference series (Wang 2008a,b).

Given the realities of the IGRA dataset, the PMF algorithm, which works without a reference series, was selected to detect the significant (95% significant F test) changepoints in the monthly BLH series at a specific observation time. PMF is proposed for detecting undocumented mean shifts that are not accompanied by any sudden change in the linear trend of the time series. PMF aims to even out the uneven distribution of false alarm rate and detection power of the corresponding penalized maximal F test that is based on a common-trend two-phase regression model (TPR3) (Wang 2008a).We ignored the changepoints that did not pass the significance test and those that needed to be supported by input documents. Although IGRA provided metadata information for the stations, not all of the available stations were included in these metadata, and events were recorded according to the year in which they occurred, without specific dates (Dai et al. 2011). In this study, we did not use the metadata as the document fails to detect the changepoints, but these data were used to validate the detected changepoints (discussed in the next section).

The quantile-matching (QM) adjustment in RHtestsV4 was performed to make adjustments after the changepoints were found. The QM adjustment can be used to adjust a series, so that the empirical distributions of all segments in the detrended base series match each other. The adjustment value depended on the empirical frequency of the datum to be adjusted (Vincent et al. 2012; Wang and Feng 2013; Wang et al. 2010). As a result, the shape of the distribution may be adjusted, although the tests are meant to detect mean shifts; in addition, the QM adjustments could account for a seasonality of discontinuity. The annual cycle, lag-1 autocorrelation, and linear trend of the base series were estimated in tandem while accounting for all identified shifts (Wang 2008a), and the trend component estimated for the base series is preserved in the QM adjustments when they are estimated without using a reference series.

3. Results

a. Diurnal cycle of boundary layer occurrence

During the nighttime, the land surface cools at a faster rate than the atmosphere above it because the surface emits more longwave radiation, causing the temperature to increase with height above the surface. This temperature inversion depresses the turbulence between the surface and atmosphere, with the resulting stable boundary layer referred to as the SBL. After sunrise, the surface absorbs solar radiation, and the air above the surface becomes unstable. Then, turbulence and the

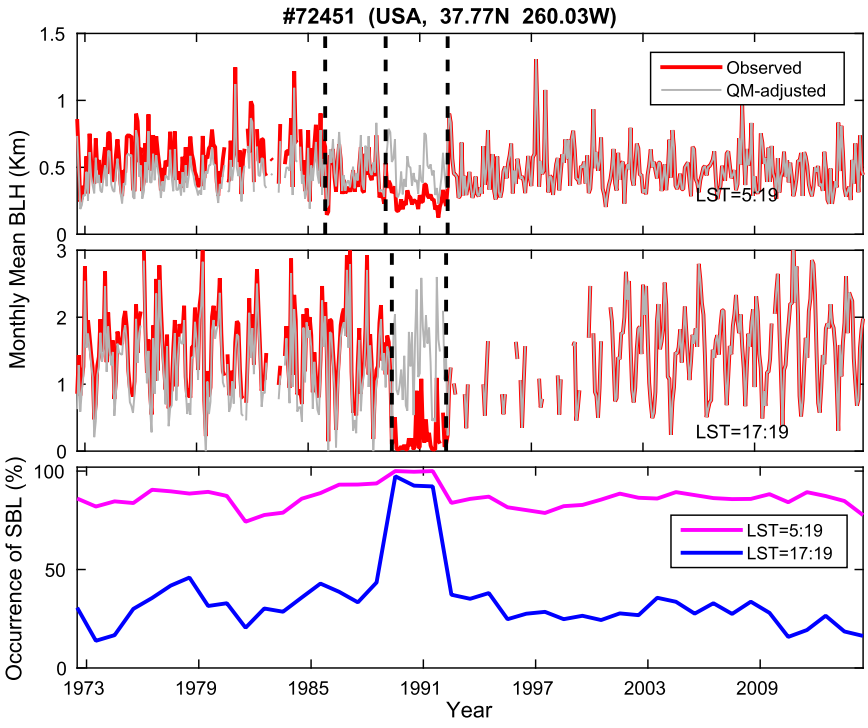

FIG. 3. Time series of monthly BLH and the frequency of SBL occurrence for U.S. station 72451 (37.77°N, 260.03°W) at its twice-daily observation times. The red line represents the raw derived BLH, and the gray line indicates the adjusted BLH series based on the method of QM adjustment. The vertical dashed line represents the detected changepoints of observed BLH based on a PMF. Changepoints in the daytime and nighttime series were both detected for 1989 and 1992, and were attributed to a change in the radiosonde model. The spurious increased frequency of occurrence of the SBL may be attributed to the false trend in the BLH.

CBL develop. However, even in the daytime, an SBL may occur over snow and ice surfaces, or when warm air is advected over a cold surface (Sun et al. 2015). As shown in Fig. 3 (bottom), CBLH was higher in daytime than at nighttime, and the frequency of SBL occurrence was lower during the daytime.

The mandatory radiosonde measurements of the World Meteorological Organization (WMO) are performed at 0000 and 1200 UTC, but a small number of soundings are obtained at other coordinated universal times (UTCs). It is difficult to derive the diurnal variation of boundary layer development based on twice-daily observations at each station. In this study, we used data from the two most frequent observation times at each station and calculated the long-term annual or seasonal frequency of occurrence of the SBL at all stations, at the two available observation times. Accordingly, for each station, we obtained two SBL (annual or seasonal) frequencies at two specific local observation times. The times of 0000 and 1200 UTC at all available stations could be converted to different local times that were used to reveal the daily variation in SBL occurrence.

Figure 4 shows the diurnal cycle of the frequency of SBL occurrence, which can indicate the development of a daily boundary layer (the occurrence of the CBLH is shown in Fig. S1 in the supplemental material). The figure shows a significant diurnal cycle of the frequency of occurrence of the SBL, with a higher frequency of 80%–100% at nighttime and a low frequency of less than 20% at 1300–1400 local solar time (LST; hereafter all times given are LST).

The daily convective boundary layer developed more rapidly at low latitudes (40°S–40°N) than at high latitudes. At low latitudes, no significant seasonal difference was observed in the daily cycle of SBL occurrence, with the development starting at approximately 2030 and ending at 0630 the next morning (with an SBL frequency exceeding 60%). However, at high latitudes, the annual mean SBL development started at 1930 and ends at 0730, with a later starting time and earlier ending time in the warm season. A much more frequent SBL occurred in the cold season, and the frequency increased as the latitude increases. In the summer, the frequency of the occurrence of the SBL increased with latitude in the

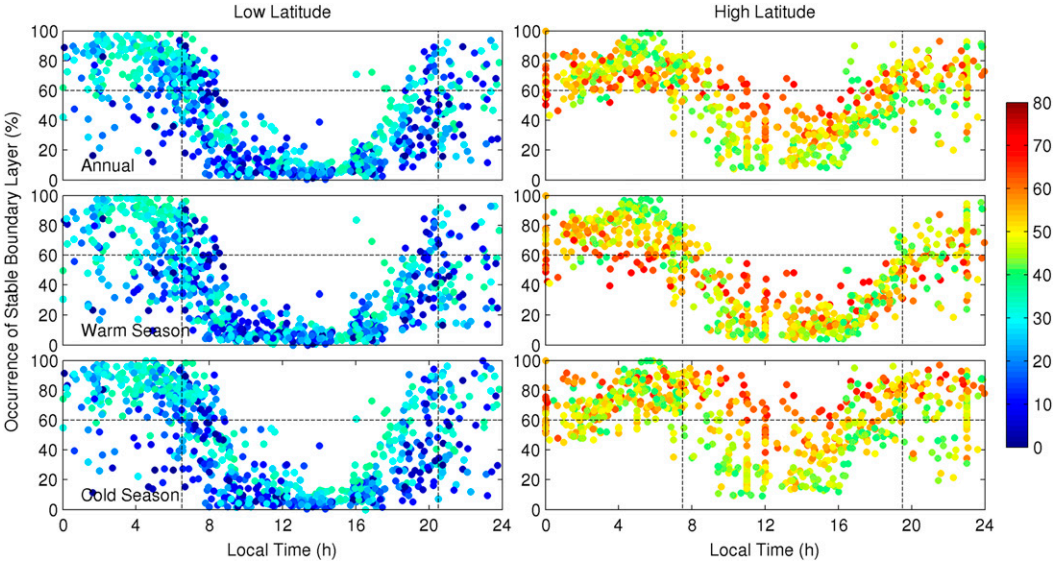

FIG. 4. Seasonal diurnal cycle of the probability of occurrence of the SBL for (left) low latitudes (40°S–40°N) and (right) high latitudes (south of 40°S and north of 40°N). The color bar indicates the latitude of each station. The vertical dashed line represents the estimated local time corresponding to an SBL frequency of 60% and indicating the dividing line between day and night. The boreal warm season is from May to October in the Northern Hemisphere and from November to April of the next year in the Southern Hemisphere. The daily launch times of the radiosonde observations are at 0000 and 1200 UTC, although a small number of soundings were obtained at other UTCs. The frequencies of occurrence of the SBL at all stations are presented at their two most frequent local observation times. The daily development of the boundary layer displays significant seasonal and zonal differences at high latitudes, with a higher frequency of SBL and a longer duration of daily SBL noted in the cold season and at higher latitudes.

daytime and decreased with latitude during the nighttime, because of the uninterrupted daylight at high latitudes. Figure S2 in the supplemental material shows the location of the stations in Fig. 4, where the SBL frequency was less than 50% from 2200 to 0700. Except for several stations in China, most stations were located on islands or in coastal areas. At these locations, the surface wind shear is stronger because of the change in the underlying surface between ocean and land. The activities of the summer monsoon may have contributed to the lower nighttime SBL frequency in summer on the west coasts of India and Australia.

Given the seasonal diurnal cycle of SBL development, we defined the daytime in the low latitudes as the period from 0630 to 2030 (without a seasonal difference), and the annual daytime at high latitudes as the period from 0730 to 1930, with a half-hour extension in the evening and morning in the warm season and a similar reduction in the cold season (i.e., 0700–2000 for the warm season and 0800–1900 for the cold season). In this study, we separated the station data into daytime and nighttime subsets according to the diurnal cycle of the SBL. Figure S3 in the supplemental material shows the observation time for all the available IGRA stations. The daytime period we defined was not symmetric around the local noon and was not equal to 12 h. Thus, for some stations, both of the two observation times were defined as daytime or nighttime, as shown in Fig. S3 in the supplemental material. In this case, we combined the two observations with their individual normalized anomaly series to derive the tendency of the BLH variation for the station.

b. *Performance of the homogenization method*

We verified the homogenized BLH time series in two steps. 1) The changepoints we detected in the BLH time series were rechecked with the metadata. If the software-detected changepoints were consistent with the changes in the measuring instruments and data processing methods, we concluded that the RHtestsV4 results were acceptable. 2) We correlated the BLH time series before and after homogenization with the BLH from the reanalysis data. If the correlation coefficients for the relationship between the homogenized BLH and reanalysis BLH were more satisfactory than those for the raw data, we concluded that our homogenized BLH time series were reliable and valid, although the reanalyzed BLH dataset was not of sufficient quality to be acceptable as reference data.

Figure 5 shows that approximately 110 stations were found to have discontinuity problems in 1992. The

periods of 1989/90 and 1986 also had frequent changepoints. Because some radiosonde sensors were sensitive to sunlight and temperature, the daytime and nighttime observations had different biases (Elliott and Gaffen 1991; Gaffen et al. 1991). Accordingly, the changepoints detected in the daytime BLH series may not be completely consistent with those of the nighttime series at a specific station. If either the daytime or nighttime BLH was detected as an inhomogeneity, the station was marked by a changepoint in the specific year. In all, 291 of the 846 stations had a homogenous BLH series (i.e., both the daytime and nighttime BLH series were homogenous).

Figure 6 shows the location of stations with changepoints for the above three periods (i.e., 1986, 1989/90, and 1992). The spatially continuous distribution of stations with changepoints in the same year, indicating the replacement or upgrade of sounding systems, occurred at approximately the same time throughout the entire country. Most of the stations found to have breakpoints were U.S. stations. Based on the station metadata information and existing publications (Elliott and Gaffen 1991; Gaffen 1994), stations in the United States changed their computers from the original ''mini-computer system'' to a ''mini-art 2 system'' and began to use a new radiation correction method and sonde model in 1986. Subsequently, during 1989/90, most of the U.S. stations changed the mini-art 2 system to a ''micro-art system,'' but a coding error occurred during this conversion at some stations that resulted in temperature values being incorrectly divided by 100 (Elliott et al. 1998). In addition, the U.S. National Weather Service switched from VIZ Manufacturing type A to type B radiosonde models in 1989. The new sonde model used a different parallel resistor in the humidity circuit, but the value of the resistor was not changed in the software until 1993, when a new sonde model (unspecified) was used (Wade 1994). Low-temperature- and low-humidity-cutoff policies were also changed in 1993, at the request of data users (Elliott et al. 1998).

The United Kingdom and some other European countries replaced their original radiation correction with a new method and changed the old sonde model (e.g., the British Kew Mark III for the United Kingdom and the Mesural for France) to the Vaisala RS80 between 1989 and 1990 (Gaffen 1993). Simultaneously, manual computers at stations in India were replaced with computers based on a semiautomatic method (Gaffen 1993). No obvious discontinuity was found in the BLH series of stations over South Africa, Australia, and Asia.

We then correlated the raw and homogenized monthly daytime BLH time series with those from the

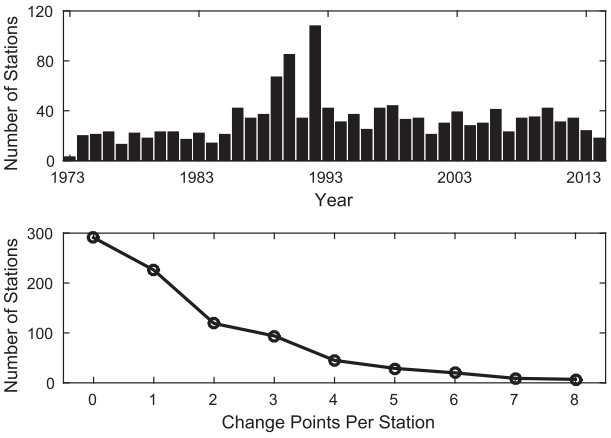

FIG. 5. (top) Time series of BLH changepoints and (bottom) the number of changepoints at each station. Monthly daytime and nighttime BLH series at 846 stations were obtained. A station was considered to show a discontinuity in a specific year if either its daytime or nighttime series had a changepoint. Approximately 110 stations were found to have a discontinuity in 1992, and the periods of 1989/90 and 1986 also contained frequent changepoints.

reanalysis data. Monthly European Centre for Medium-Range Weather Forecasts interim reanalysis (ERA-Interim; 0.5° resolution) and the Modern-Era Retrospective Analysis for Research and Applications, version 2 (MERRA-2; ½° × ⅔° latitude–longitude resolution), BLH dataset from 1979 to 2014 were used to verify the performance of the homogenization. The BLH in the MERRA-2 dataset was estimated based on vertical profiles of the diffusion coefficient with the Goddard Earth Observing System Model, version 5 (GEOS-5), and Data Assimilation System (DAS) (Jordan et al. 2010). The mixed layer height in ERA-Interim was determined using an entraining parcel, and by selecting the top of the stratocumulus or cloud base in shallow convection situations (Dee et al. 2011).

As shown in Fig. S4 in the supplemental material, there was a better agreement between these two kinds of reanalysis datasets in the daytime BLH than in the nighttime. In addition, because of the difficulty in modeling SBLH (Sun et al. 2015), only the daytime BLH was compared between the reanalysis and observed BLH. There was a good consistency between the daytime homogenized BLH series and the reanalysis BLH as shown in Fig. 7, with a significant correlation coefficient (>0.7) over much of Europe and the United States. As shown in Fig. 7, in 343 of the 739 stations, a significant changepoint was detected during the study period. For the stations with an inhomogeneous BLH series, 60% of them had an improved correlation coefficient or statistical significance with the reanalysis BLH after homogenization

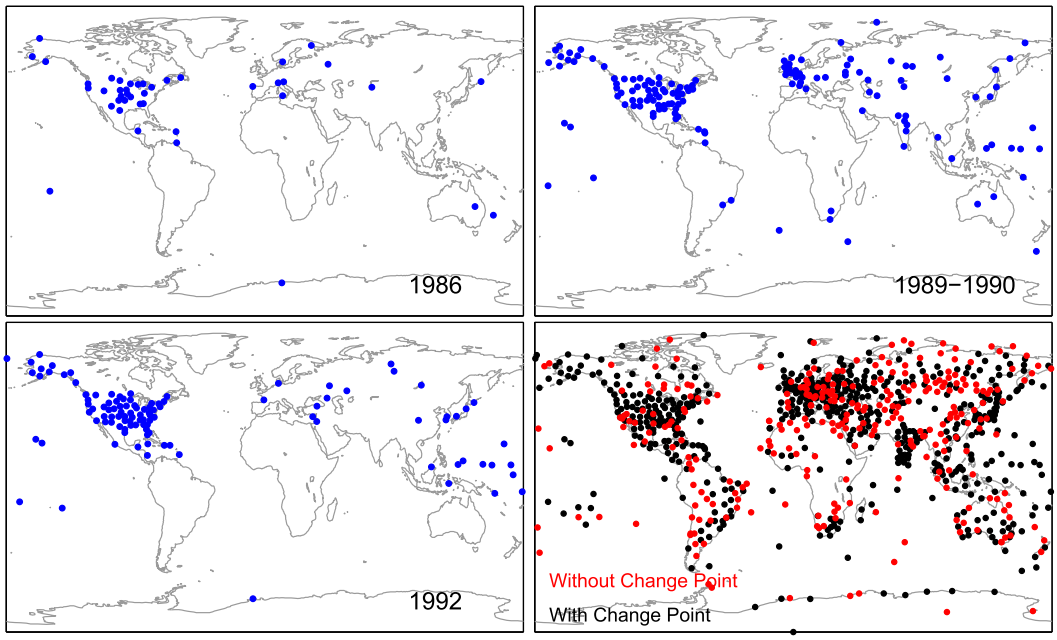

FIG. 6. Location of stations with changepoints in 1986, 1989/90, and 1992 and those with/without changepoints during the study period. In all, 291 of the 846 stations had homogeneous raw BLH series. Most of the stations detected with changepoints were U.S. stations. The United Kingdom and some other European countries had discontinuous BLH data in 1989/90. Some stations over South Africa, Australia, and Asia did not have discontinuous BLH.

(202/343 stations for ERA-Interim and 205/343 stations for MERRA-2). The effect of homogenization was more significant in the United States than in the other regions, with an obvious improvement of the correlation coefficient with the reanalysis data. Both the improved correlation coefficient and statistical significance support the validity of the homogenization method.

The correlation between simulated and observed BLH was weak over low latitudes and the east coast of the United States. The inconsistency between ERA-Interim and MERRA-2 BLH over the east coast of the United States and Southeast Asia is likely because of the difficulty of models simulating boundary layer processes over these regions (Fig. S4 in the supplemental material), which explains the low correlation coefficients between the observed BLH and reanalysis series over these regions. The weak correlation between the radiosonde-derived BLH and those of the reanalysis over low-latitude regions can be attributed to the frequency of convection cloud in equatorial areas. The effect of boundary layer cloud on the development of turbulence depended on the temperature stratification of the cloud (i.e., the top of the boundary layer was located at the height of the strongest inversion in the cloud rather than the top of the stratocumulus, or the cloud base in shallow convection as that in numerical models) (Wang and Wang 2014). Current reanalyses still experience difficulties in accurately simulating clouds (Wang et al. 2015).

c. *Trends in convective and stable BLH*

As shown in Fig. 4, the CBLH was dominant during the daytime and the SBLH occurred frequently at night; therefore, we present the variability in daytime CBLH and nighttime SBLH in this section, to evaluate the effect of homogenization and estimate the long-term variability of BLH. To reduce the effects of the diurnal cycle of the BLH and its latitudinal variation (Fetzer et al. 2004; Ratnam et al. 2010; Seidel et al. 2012), we used the normalized anomaly of BLH in this section. This normalization was in reference to the climatology of each station, at its specific observation time, and was used to facilitate an analysis of the station's daytime or nighttime variation tendency.

Figure 8 presents a detailed comparison of the raw-derived and homogenized (QM adjusted) BLH variation tendencies, at station scales, during 1973–2014. Both raw and homogenized daytime CBLH displayed an increasing tendency during the study period, whereas in contrast the nighttime SBLH had a decreasing tendency. The global daytime CBLH trend changed little before and after homogenization, with an increasing trend of 1.6% decade^{-1}. The nighttime homogenized SBLH decreased by −4.2% decade^{-1} compared to a

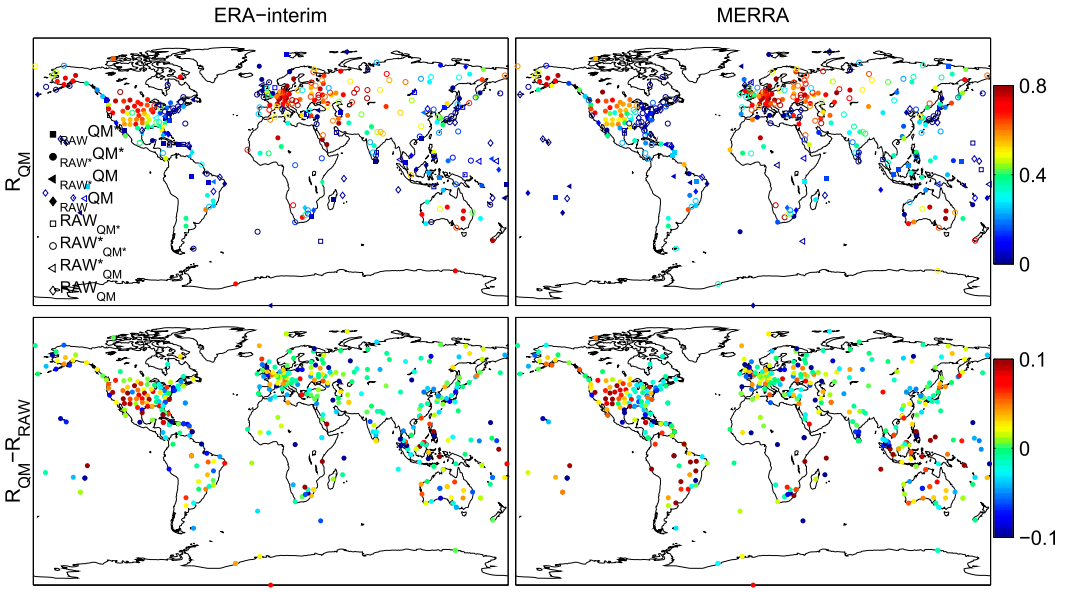

FIG. 7. (top) Correlation coefficients between daytime homogenized monthly BLH and reanalysis BLH from (left) ERA-Interim and (right) MERRA-2. (bottom) Correlation coefficients for the difference between QM-adjusted BLH with reanalysis dataset and raw BLH with reanalysis dataset. Daily (i.e., four times per day) ERA-Interim (0.5° resolution) and monthly 24-h MERRA-2 ($1/2° \times 2/3°$ latitude–longitude resolution) BLH data from 1979 to 2014 were used to calculate the monthly daytime series. Only the IGRA stations with changepoints detected are shown. The circles in the top indicate that both the raw and QM-adjusted BLH were significantly correlated (95% significance level), with the reanalysis BLH. The squares and triangles indicate that the homogenized or raw BLH had significant correlations with the reanalysis BLH, respectively. Diamonds indicate that both the homogenized and raw BLH had a poor correlation with the reanalysis BLH. Solid (open) markers represent higher (lower) correlation coefficients between QM-adjusted and reanalysis BLH than those for raw BLH. Among the daytime stations, 343 of 739 had significant changepoints, and 60% of the them had an improved correlation coefficient or statistical significance (i.e., the first to fifth kinds of markers in the top) with the reanalysis BLH after homogenization (202/343 stations for ERA-Interim and 205/343 stations for MERRA-2).

decrease of −7.1% decade^{-1} based on the raw series. The shallow stable boundary layers, with lower SBLH values, were more sensitive to the adjustment (i.e., a larger relative variability with the same magnitude of adjustment, which contributed to the significant difference in the SBLH trend before and after homogenization). In addition, more stations displayed a significant variation tendency after homogenization; for example, for the daytime CBLH case, 333 and 381 stations had significant linear trends before and after homogenization, respectively, which also implied that the homogenization process effectively removed the breakpoints from the raw BLH data.

Based on the distribution of stations, six subregions were defined to show their regionally averaged BLH variations. To minimize the effect of missing data and climatology, the normalized annual BLH anomalies of each station were averaged on the regional scale. Figure 9 shows the locations of the six subregions and their daytime CBLH and nighttime SBLH trends. The most significant influence of the inhomogeneous BLH appeared in the United States. As at the U.S. station shown in Fig. 3, the occurrence of a daytime SBL increased dramatically during 1991–93, thus, there were almost no records of a daytime CBL at that time over the United States (Fig. 9). The raw SBLH series showed an abrupt decrease during 1991–93 in the United States, with a −7.3% decade^{-1} decrease during the study period. The homogenization effectively removed the discontinuity in the raw nighttime SBLH series over the United States, and revealed a significant decreasing tendency of −6.9% decade^{-1} (statistically significant at the 95% significant level or greater). The difference between raw and homogenized global SBLH could be attributed to the moderate decreasing tendency of SBLH after homogenization over Europe, Australia, and the United States. The effects of homogenization were less significant for the regional daytime CBLH. The homogenized daytime CBLH increased significantly by 2.8%, 0.9%, 1.6%, and 2.7% decade^{-1} over Europe, the United States, Japan, and Australia, respectively, with almost same pattern with those based on raw observed CBLH. High-vertical-resolution data in China have been available since 1998. The daytime

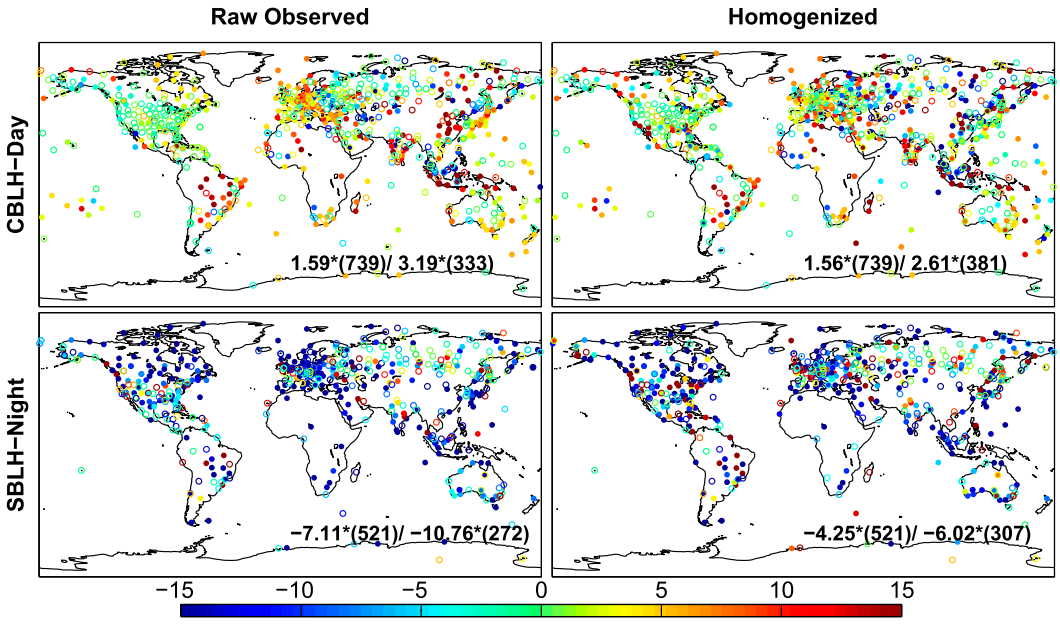

FIG. 8. Spatial distributions of the linear trends (% decade^{-1}) of (left) observed and (right) QM-adjusted daytime CBLH and nighttime SBLH from 1973 to 2014. Solid circles indicate the trends that are statistically significant at the 95% significance level or greater. Global averaged normalized annual BLH anomaly series are shown in Fig. S5 in the supplemental material, and its linear trends are presented here in each panel, with a format showing the global mean trend of all available stations (number of stations)/global trend based on the stations with significant trend (number of stations with significant trend). Both the raw and homogenized daytime CBLH exhibited positive trends, whereas the nighttime SBLH decreased from 1973 to 2014.

CBLH has also increased in China, and the nighttime SBLH decreased recently. There was no obvious long-term tendency of BLH in Russia, which may be attributed to its larger span of longitude, with different underlying surface types.

4. Conclusions and discussion

As the most common source of atmospheric BLH, the IGRA dataset from 1973 to 2014 released by the NCDC were used to examine the long-term variability of global BLH. We found that the raw data of radiosonde-derived BLH included marked inhomogeneities. PMF and QM adjustment in the RHtestsV4 package were used to detect the changepoints and adjust the observed BLH series. The most significant inhomogeneity in the derived BLH time series was found over the United States from 1986 to 1992, when the meteorological measuring system was upgraded.

The convective boundary layer (CBL) is dominant during the daytime and a more frequent stable boundary layer (SBL) occurs at night. The homogenization did not significantly change the magnitude of the daytime CBLH tendency, but it did improve the confidence of the linear trend. The trend of nighttime SBLH tended to be more moderate after homogenization because of the small magnitude of SBLH and its sensitivity to adjustment. Both the raw and homogenized daytime CBLH displayed an increasing tendency during 1973–2014, with almost the same global average of about 1.6% decade^{-1}; however, the homogenized global nighttime SBLH decreased by −4.3% decade^{-1} compared to the raw observation of −7.1% decade^{-1}. Regionally, the homogenized daytime CBLH increased by 2.8%, 0.9%, 1.6%, and 2.7% decade^{-1} over Europe, the United States, Japan, and Australia, respectively. The nighttime SBLH decreased consistently, with significant decreases of −2.7%, −6.9%, −7.7%, and −3.5% decade^{-1} over the four regions, respectively. The increasing trend of BLH found in Europe was consistent with those reported by Zhang et al. (2013) based on an independent BLH estimation method.

The development of the boundary layer is determined by large-scale circulation and local land–atmosphere interactions (i.e., thermodynamic and dynamic conditions). The local land–atmosphere interaction could be partly quantified using the available radiosonde dataset (i.e., the vertical gradients of near-surface air temperature and wind speed). Wind (U, V) information was only available at mandatory pressure levels (e.g., 1000, 925,

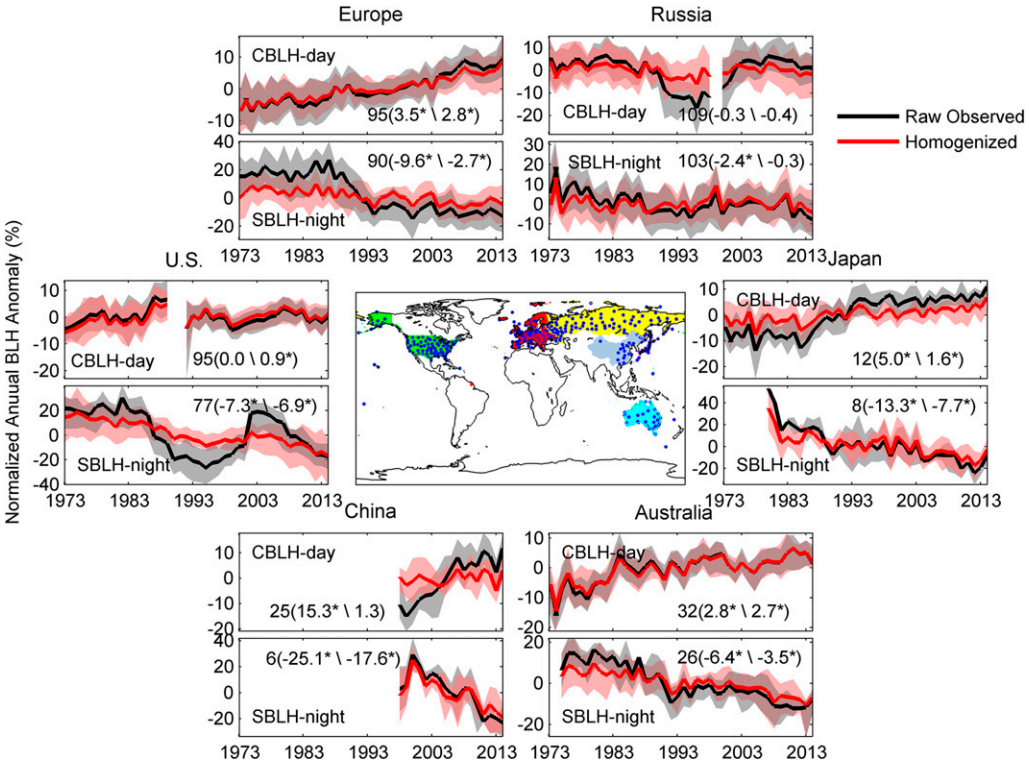

FIG. 9. Time series of the regional daytime CBLH and nighttime SBLH. The black line represents the raw observations of BLH, and the red line indicates the homogenized result. The shaded area indicates the 25%–75% percentile of the regional annual BLH. The number in each panel indicates the sample size of each subregion, followed by the linear trends of raw observed and homogenized series (% decade^{-1}). The asterisk following the trend indicates the linear trends that are statistically significant at the 95% significance level or greater. Only the time periods with effective samples exceeding 50% are shown here.

850, 700, and 500 hPa) at most stations. For this reason, to maintain the consistency of the day and night, we only used the vertical gradients of temperature and wind shear between the lowest two available mandatory pressure levels (upper level minus lower level) to discuss the mechanism driving the BLH trends. The monthly anomalies of temperature gradient and wind shear were used to avoid the effects of the annual and seasonal cycles of meteorological variables. We found that the thermodynamic effects differed during the daytime and nighttime (i.e., a positive correlation was noted between daytime BLH and temperature gradient, whereas the opposite correlation was observed at nighttime). As shown in Fig. 10, a strong vertical gradient of temperature (i.e., strong negative gradient) in the daytime reflects unstable stratification, and this instability can stimulate turbulence in the boundary layer. Near-surface thermal inversion or at least stable stratification (i.e., a weak negative or even positive temperature gradient) occurs very frequently at night. A steady inversion near Earth's surface indicates a deep SBL. Thus, the results showed a positive correlation between the temperature gradient and nighttime BLH. Additionally, both daytime and nighttime BLH were positively correlated with wind shear because of its momentum transfer for the development of turbulence, but the effect of wind shear was more significant at night.

The trends of CBLH and SBLH were determined by different parameters. No single parameter can provide a sufficient explanation. The reported increasing trend of atmospheric downward longwave radiation is generally consistent with the increasing CBLH and decreasing SBLH over the global land surface (Wang and Dickinson 2013; Wang et al. 2009). The increasing trend of CBLH over Europe and Japan was consistent with the reported increases in surface solar radiation in these regions (Wang et al. 2012b; Wild 2009). However, the changes in surface solar radiation in China, the United States, and Australia cannot explain the increasing trend in CBLH in these regions. In addition to the energy input, the partitioning of the surface net radiation into surface latent heat flux and sensible heat fluxes is an important factor determining the variability of BLH. Previous studies have reported that the RH has

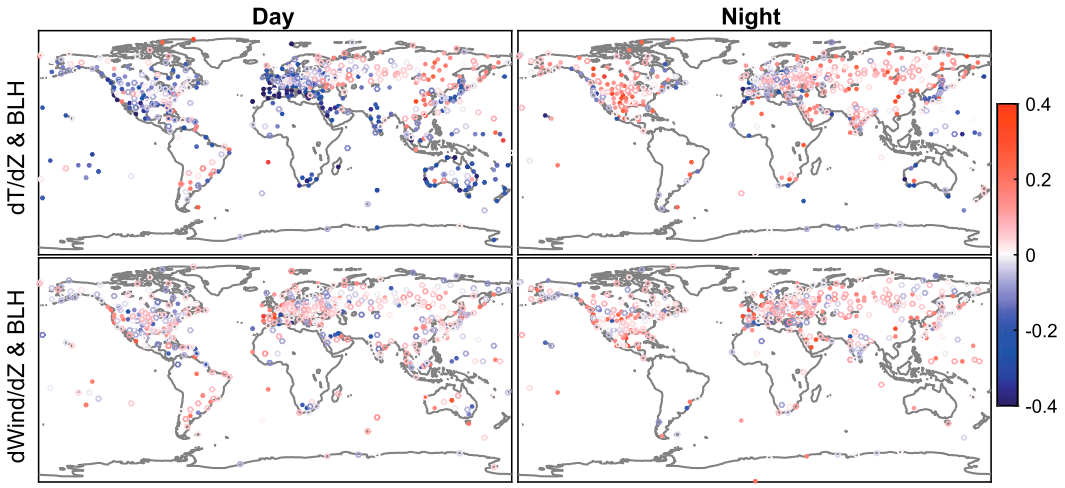

FIG. 10. Correlation coefficients of monthly anomaly QM-adjusted BLH, with the (top) near-surface temperature vertical gradient and (bottom) wind shear. Solid circles indicate a significant correlation at the 95% significance level or greater. To avoid the effects of annual and seasonal cycles of meteorological variables, monthly anomalies were used to calculate the correlation coefficients. Wind (U, V) information was only available at mandatory pressure levels (e.g., 1000, 925, 850, 700, and 500 hPa) at most stations. Therefore, to maintain the consistency of the day and night, we only used the vertical gradients of temperature and wind shear between the lowest two available mandatory pressure levels (upper minus lower level) to discuss the mechanism governing the BLH tendency (i.e., the two pressure levels selected may be different for all stations, but are the same for a specific station). The thermodynamic effect differed during the daytime and nighttime (i.e., a positive correlation occurred between the daytime BLH and the temperature gradient, but the opposite pattern was observed at nighttime). Both daytime and nighttime BLH were positively correlated with the wind shear because of its momentum transfer for the development of turbulence.

decreased in recent decades (Simmons et al. 2010; Wang et al. 2012a), indicating more surface energy has been partitioning into the sensible heat flux. This change implies that land heating has increased, which is in general agreement with the increased CBLH.

Radiosonde observations have been proven to experience inhomogeneity issues. Existing studies of the inhomogeneity of radiosonde data have focused on the absolute values of temperature, humidity, or wind fields. These studies have shown that a more frequent inhomogeneity occurs in the upper levels of radiosonde data (i.e., the upper troposphere and stratosphere) than the lower levels, which are used to derive BLH (Dai et al. 2011; Elliott and Gaffen 1991; Elliott et al. 1998). Furthermore, all the existing homogenization methods were operated using absolute values of temperature and humidity variables at the mandatory pressure levels, that is, 1000, 850, 700, 500, 400, 300, 250, 200, 150, 100, 70, 50, 30, 20, and 10 hPa. These data are too coarse to derive a reliable estimation of BLH. We therefore first calculated daily BLH from the raw radiosonde data at the original vertical resolution archived by IGRA, and then homogenized the monthly BLH time series. We found that BLH derived from a lower level radiosonde dataset also had a significant inhomogeneity and should be addressed.

This study represents the first attempt to homogenize the radiosonde-derived BLH using the PMF and QM adjustment procedures in the RHtests package. Significant changepoints were detected at most stations. This finding can be explained in terms of the metadata and the well-known improvements in observation methods. We used a two-step procedure to verify our homogenization results. Both steps confirmed that the homogenization substantially improved the quality of the BLH time series. However, the QM-adjusted method was based on the assumption that BLH differences before and after the changepoints were entirely attributable to nonclimatic changes, which is largely true in most cases. We cannot exclude cases where nonlinear trends and other natural variations alter BLH. The detection of break points is possible with the RHtestsV4 package when a homogenous reference series is not available. However, the results need intensive analysis (Wang and Feng 2013), and the lack of a reference dataset of radiosonde-derived BLH makes it more difficulty to verify the performance of BLH homogenization. Long-term lidar and GPS datasets may be a good reference series for the validation of the homogenized BLH. However, these remote sensing datasets are sparsely available and have very short time scales (Ao et al. 2012;

Liu et al. 2015; Luo et al. 2014; Z. Wang et al. 2012; Xie et al. 2006).

In this study, we defined 0630–2030 and 0730–1930 LST as daytime in the low and high latitudes, respectively; however, the common definitions of daytime and nighttime are based on the solar elevation angle, local latitude, and longitude. Therefore, we also used the National Oceanic and Atmospheric Administration (NOAA) method (http://www.esrl.noaa.gov/gmd/grad/solcalc/sunrise.html) to define day and night, and then to estimate the regional variation of BLH. As shown in Fig. S6 in the supplemental material, based on the NOAA day and night definitions, the regionally averaged BLH variation did not display significant differences from that based on the daily cycle of the SBL. However, using the NOAA definitions, most stations over the United States and China were excluded (the number of regionally available stations is shown in Fig. S6 in the supplemental material) because their observation times were near sunset and sunrise. In addition, the SBL will not disappear immediately at sunrise and also will not develop immediately at sunset. Thus, we used a day/night definition based on the daily cycle of the SBL in this study.

Acknowledgments. This study was funded by the National Natural Science Foundation of China (41525018 and 91337111) and the National Basic Research Program of China (2012CB955302). The radiosonde data used in this study were provided by the National Climatic Data Center (ftp://ftp.ncdc.noaa.gov/pub/data/igra/). The RHtestsV4 package used to homogenize the BLH was an R program downloaded from the Expert Team on Climate Change Detection and Indices (ETCCDI) website (http://etccdi.pacificclimate.org/software.shtml), with the help of Dr. Xiaolan Wang and Yang Feng. We thank the editor and the three anonymous reviewers for comments and suggestions.

REFERENCES

Ao, C. O., D. E. Waliser, S. K. Chan, J. L. Li, B. Tian, F. Xie, and A. J. Mannucci, 2012: Planetary boundary layer heights from GPS radio occultation refractivity and humidity profiles. *J. Geophys. Res.*, **117**, D16117, doi:10.1029/2012JD017598.

Chan, K. M., and R. Wood, 2013: The seasonal cycle of planetary boundary layer depth determined using COSMIC radio occultation data. *J. Geophys. Res. Atmos.*, **118**, 12 422–12 434, doi:10.1002/2013JD020147.

Dai, A., J. Wang, P. W. Thorne, D. E. Parker, L. Haimberger, and X. L. Wang, 2011: A new approach to homogenize daily radiosonde humidity data. *J. Climate*, **24**, 965–991, doi:10.1175/2010JCLI3816.1.

Dee, D. P., and Coauthors, 2011: The ERA-Interim reanalysis: Configuration and performance of the data assimilation system. *Quart. J. Roy. Meteor. Soc.*, **137**, 553–597, doi:10.1002/qj.828.

Durre, I., and X. Yin, 2008: Enhanced radiosonde data for studies of vertical structure. *Bull. Amer. Meteor. Soc.*, **89**, 1257–1262, doi:10.1175/2008BAMS2603.1.

——, R. S. Vose, and D. B. Wuertz, 2006: Overview of the Integrated Global Radiosonde Archive. *J. Climate*, **19**, 53–68, doi:10.1175/JCLI3594.1.

——, ——, and ——, 2008: Robust automated quality assurance of radiosonde temperatures. *J. Appl. Meteor. Climatol.*, **47**, 2081–2095, doi:10.1175/2008JAMC1809.1.

Elliott, W. P., and D. J. Gaffen, 1991: On the utility of radiosonde humidity archives for climate studies. *Bull. Amer. Meteor. Soc.*, **72**, 1507–1520, doi:10.1175/1520-0477(1991)072<1507:OTUORH>2.0.CO;2.

——, R. J. Ross, and B. Schwartz, 1998: Effects on climate records of changes in National Weather Service humidity processing procedures. *J. Climate*, **11**, 2424–2436, doi:10.1175/1520-0442(1998)011<2424:EOCROC>2.0.CO;2.

Eresmaa, N., A. Karppinen, S. M. Joffre, J. Räsänen, and H. Talvitie, 2006: Mixing height determination by ceilometer. *Atmos. Chem. Phys.*, **6**, 1485–1493, doi:10.5194/acp-6-1485-2006.

Ferrero, L., A. Riccio, M. G. Perrone, G. Sangiorgi, B. S. Ferrini, and E. Bolzacchini, 2011: Mixing height determination by tethered balloon-based particle soundings and modeling simulations. *Atmos. Res.*, **102**, 145–156, doi:10.1016/j.atmosres.2011.06.016.

Fetzer, E. J., J. Teixeira, E. T. Olsen, and E. F. Fishbein, 2004: Satellite remote sounding of atmospheric boundary layer temperature inversions over the subtropical eastern Pacific. *Geophys. Res. Lett.*, **31**, L17102, doi:10.1029/2004GL020174.

Gaffen, D. J., 1993: Historical changes in radiosonde instruments and practices. WMO/TD-No. 541, 123 pp. [Available online at http://library.wmo.int/pmb_ged/wmo-td_541_en.pdf.]

——, 1994: Temporal inhomogeneities in radiosonde temperature records. *J. Geophys. Res.*, **99**, 3667–3676, doi:10.1029/93JD03179.

——, T. P. Barnett, and W. P. Elliott, 1991: Space and time scales of global tropospheric moisture. *J. Climate*, **4**, 989–1008, doi:10.1175/1520-0442(1991)004<0989:SATSOG>2.0.CO;2.

Garratt, J. R., 1993: Sensitivity of climate simulations to land-surface and atmospheric boundary-layer treatments—A review. *J. Climate*, **6**, 419–448, doi:10.1175/1520-0442(1993)006<0419:SOCSTL>2.0.CO;2.

——, 1994: *The Atmospheric Boundary Layer.* Cambridge University Press, 316 pp.

Glickman, T. S., 2000: *Glossary of Meteorology.* Amer. Meteor. Soc., 855 pp.

Gryning, S.-E., and E. Batchvarova, 2002: Marine boundary layer and turbulent fluxes over the Baltic Sea: Measurements and modelling. *Bound.-Layer Meteor.*, **103**, 29–47, doi:10.1023/A:1014514513936.

Gupta, S., R. T. McNider, M. Trainer, R. J. Zamora, K. Knupp, and M. P. Singh, 1997: Nocturnal wind structure and plume growth rates due to inertial oscillations. *J. Appl. Meteor.*, **36**, 1050–1063, doi:10.1175/1520-0450(1997)036<1050:NWSAPG>2.0.CO;2.

Haimberger, L., 2007: Homogenization of radiosonde temperature time series using innovation statistics. *J. Climate*, **20**, 1377–1403, doi:10.1175/JCLI4050.1.

——, C. Tavolato, and S. Sperka, 2012: Homogenization of the global radiosonde temperature dataset through combined comparison with reanalysis background series and neighboring stations. *J. Climate*, **25**, 8108–8131, doi:10.1175/JCLI-D-11-00668.1.

Hennemuth, B., and A. Lammert, 2006: Determination of the atmospheric boundary layer height from radiosonde and lidar

backscatter. *Bound.-Layer Meteor.*, **120**, 181–200, doi:10.1007/s10546-005-9035-3.

Hong, S.-Y., and H.-L. Pan, 1998: Convective trigger function for a mass-flux cumulus parameterization scheme. *Mon. Wea. Rev.*, **126**, 2599–2620, doi:10.1175/1520-0493(1998)126<2599:CTFFAM>2.0.CO;2.

Johansson, C., A.-S. Smedman, U. Högström, J. G. Brasseur, and S. Khanna, 2001: Critical test of the validity of Monin–Obukhov similarity during convective conditions. *J. Atmos. Sci.*, **58**, 1549–1566, doi:10.1175/1520-0469(2001)058<1549:CTOTVO>2.0.CO;2.

Jordan, N. S., R. M. Hoff, and J. T. Bacmeister, 2010: Validation of Goddard Earth Observing System-version 5 MERRA planetary boundary layer heights using *CALIPSO*. *J. Geophys. Res.*, **115**, D24218, doi:10.1029/2009JD013777.

Lee, S.-J., and H. Kawai, 2011: Mixing depth estimation from operational JMA and KMA wind-profiler data and its preliminary applications: Examples from four selected sites. *J. Meteor. Soc. Japan*, **89**, 15–28, doi:10.2151/jmsj.2011-102.

Lewis, J. R., E. J. Welton, A. M. Molod, and E. Joseph, 2013: Improved boundary layer depth retrievals from MPLNET. *J. Geophys. Res. Atmos.*, **118**, 9870–9879, doi:10.1002/jgrd.50570.

Liu, J., J. Huang, B. Chen, T. Zhou, H. Yan, H. Jin, Z. Huang, and B. Zhang, 2015: Comparisons of PBL heights derived from *CALIPSO* and ECMWF reanalysis data over China. *J. Quant. Spectrosc. Radiat. Transfer*, **153**, 102–112, doi:10.1016/j.jqsrt.2014.10.011.

Liu, S., and X.-Z. Liang, 2010: Observed diurnal cycle climatology of planetary boundary layer height. *J. Climate*, **23**, 5790–5809, doi:10.1175/2010JCLI3552.1.

Luo, T., R. Yuan, and Z. Wang, 2014: Lidar-based remote sensing of atmospheric boundary layer height over land and ocean. *Atmos. Meas. Tech.*, **7**, 173–182, doi:10.5194/amt-7-173-2014.

McCarthy, M. P., H. A. Titchner, P. W. Thorne, S. F. B. Tett, L. Haimberger, and D. E. Parker, 2008: Assessing bias and uncertainty in the HadAT-adjusted radiosonde climate record. *J. Climate*, **21**, 817–832, doi:10.1175/2007JCLI1733.1.

——, P. W. Thorne, and H. A. Titchner, 2009: An analysis of tropospheric humidity trends from radiosondes. *J. Climate*, **22**, 5820–5838, doi:10.1175/2009JCLI2879.1.

Parker, D. E., and D. I. Cox, 1995: Towards a consistent global climatological rawinsonde data-base. *Int. J. Climatol.*, **15**, 473–496, doi:10.1002/joc.3370150502.

Pattantyús-Ábrahám, M., and W. Steinbrecht, 2015: Temperature trends over Germany from homogenized radiosonde data. *J. Climate*, **28**, 5699–5715, doi:10.1175/JCLI-D-14-00814.1.

Ratnam, M. V., M. S. Kumar, G. Basha, V. K. Anandan, and A. Jayaraman, 2010: Effect of the annular solar eclipse of 15 January 2010 on the lower atmospheric boundary layer over a tropical rural station. *J. Atmos. Sol. Terr. Phys.*, **72**, 1393–1400, doi:10.1016/j.jastp.2010.10.009.

Schmid, P., and D. Niyogi, 2012: A method for estimating planetary boundary layer heights and its application over the ARM Southern Great Plains site. *J. Atmos. Oceanic Technol.*, **29**, 316–322, doi:10.1175/JTECH-D-11-00118.1.

Seibert, P., F. Beyrich, S.-E. Gryning, S. Joffre, A. Rasmussen, and P. Tercier, 2000: Review and intercomparison of operational methods for the determination of the mixing height. *Atmos. Environ.*, **34**, 1001–1027, doi:10.1016/S1352-2310(99)00349-0.

Seidel, D. J., C. O. Ao, and K. Li, 2010: Estimating climatological planetary boundary layer heights from radiosonde observations: Comparison of methods and uncertainty analysis. *J. Geophys. Res.*, **115**, D16113, doi:10.1029/2009JD013680.

——, Y. Zhang, A. Beljaars, J.-C. Golaz, A. R. Jacobson, and B. Medeiros, 2012: Climatology of the planetary boundary layer over the continental United States and Europe. *J. Geophys. Res.*, **117**, D17106, doi:10.1029/2012JD018143.

Sempreviva, A. M., and S.-E. Gryning, 2000: Mixing height over water and its role on the correlation between temperature and humidity fluctuations in the unstable surface layer. *Bound.-Layer Meteor.*, **97**, 273–291, doi:10.1023/A:1002749729856.

Sherwood, S. C., C. L. Meyer, R. J. Allen, and H. A. Titchner, 2008: Robust tropospheric warming revealed by iteratively homogenized radiosonde data. *J. Climate*, **21**, 5336–5352, doi:10.1175/2008JCLI2320.1.

Simmons, A. J., K. M. Willett, P. D. Jones, P. W. Thorne, and D. P. Dee, 2010: Low-frequency variations in surface atmospheric humidity, temperature, and precipitation: Inferences from reanalyses and monthly gridded observational data sets. *J. Geophys. Res.*, **115**, D01110, doi:10.1029/2009JD012442.

Sorbjan, Z., 1989: *Structure of the Atmospheric Boundary Layer*. Prentice Hall, 317 pp.

Sun, J., and Coauthors, 2015: Review of wave–turbulence interactions in the stable atmospheric boundary layer. *Rev. Geophys.*, **53**, 956–993, doi:10.1002/2015RG000487.

Thorne, P. W., J. R. Lanzante, T. C. Peterson, D. J. Seidel, and K. P. Shine, 2011: Tropospheric temperature trends: History of an ongoing controversy. *Wiley Interdiscip. Rev.: Climate Change*, **2**, 66–88, doi:10.1002/wcc.80.

Titchner, H. A., P. W. Thorne, M. P. McCarthy, S. F. B. Tett, L. Haimberger, and D. E. Parker, 2009: Critically reassessing tropospheric temperature trends from radiosondes using realistic validation experiments. *J. Climate*, **22**, 465–485, doi:10.1175/2008JCLI2419.1.

Venema, V. K. C., and Coauthors, 2012: Benchmarking homogenization algorithms for monthly data. *Climate Past*, **8**, 89–115, doi:10.5194/cp-8-89-2012.

Vincent, L. A., X. L. Wang, E. J. Milewska, H. Wan, F. Yang, and V. Swail, 2012: A second generation of homogenized Canadian monthly surface air for climate trend analysis. *J. Geophys. Res.*, **117**, D18110, doi:10.1029/2012JD017859.

Vogelezang, D. H. P., and A. A. M. Holtslag, 1996: Evaluation and model impacts of alternative boundary-layer height formulations. *Bound.-Layer Meteor.*, **81**, 245–269, doi:10.1007/BF02430331.

von Engeln, A., and J. Teixeira, 2013: A planetary boundary layer height climatology derived from ECMWF reanalysis data. *J. Climate*, **26**, 6575–6590, doi:10.1175/JCLI-D-12-00385.1.

Wade, C. G., 1994: An evaluation of problems affecting the measurement of low relative humidity on the United States radiosonde. *J. Atmos. Oceanic Technol.*, **11**, 687–700, doi:10.1175/1520-0426(1994)011<0687:AEOPAT>2.0.CO;2.

Wang, K., and R. E. Dickinson, 2013: Global atmospheric downward longwave radiation at the surface from ground-based observations, satellite retrievals, and reanalyses. *Rev. Geophys.*, **51**, 150–185, doi:10.1002/rog.20009.

——, ——, and S. Liang, 2009: Clear sky visibility has decreased over land globally from 1973 to 2007. *Science*, **323**, 1468–1470, doi:10.1126/science.1167549.

——, ——, and ——, 2012a: Global atmospheric evaporative demand over land from 1973 to 2008. *J. Climate*, **25**, 8353–8361, doi:10.1175/JCLI-D-11-00492.1.

——, ——, M. Wild, and S. Liang, 2012b: Atmospheric impacts on climatic variability of surface incident solar radiation. *Atmos. Chem. Phys.*, **12**, 9581–9592, doi:10.5194/acp-12-9581-2012.

——, Q. Ma, Z. Li, and J. Wang, 2015: Decadal variability of surface incident solar radiation over China: Observations, satellite retrievals, and reanalyses. *J. Geophys. Res.*, **120**, 6500–6514, doi:10.1002/2015JD023420.

Wang, X., 2008a: Penalized maximal *F* test for detecting undocumented mean shift without trend change. *J. Atmos. Oceanic Technol.*, **25**, 368–384, doi:10.1175/2007JTECHA982.1.

——, 2008b: Accounting for autocorrelation in detecting mean shifts in climate data series using the penalized maximal *t* or *F* test. *J. Appl. Meteor. Climatol.*, **47**, 2423–2444, doi:10.1175/2008JAMC1741.1.

——, and Y. Feng, 2013: RHtestsV4 user manual. Climate Research Division, Atmospheric Science and Technology Directorate, Science and Technology Branch, Environment Canada. 28 pp. [Available online at http://etccdi.pacificclimate.org/software.shtml.]

——, and K. Wang, 2014: Estimation of atmospheric mixing layer height from radiosonde data. *Atmos. Meas. Tech.*, **7**, 1701–1709, doi:10.5194/amt-7-1701-2014.

Wang, X. L., H. Chen, Y. Wu, Y. Feng, and Q. Pu, 2010: New techniques for the detection and adjustment of shifts in daily precipitation data series. *J. Appl. Meteor. Climatol.*, **49**, 2416–2436, doi:10.1175/2010JAMC2376.1.

Wang, Z., X. Cao, L. Zhang, J. Notholt, B. Zhou, R. Liu, and B. Zhang, 2012: Lidar measurement of planetary boundary layer height and comparison with microwave profiling radiometer observation. *Atmos. Meas. Tech.*, **5**, 1965–1972, doi:10.5194/amt-5-1965-2012.

White, A. B., C. J. Senff, and R. M. Banta, 1999: A comparison of mixing depths observed by ground-based wind profilers and an airborne lidar. *J. Atmos. Oceanic Technol.*, **16**, 584–590, doi:10.1175/1520-0426(1999)016<0584:ACOMDO>2.0.CO;2.

Wild, M., 2009: Global dimming and brightening: A review. *J. Geophys. Res.*, **114**, D00D16, doi:10.1029/2008JD011470.

Xie, F., S. Syndergaard, E. R. Kursinski, and B. M. Herman, 2006: An approach for retrieving marine boundary layer refractivity from GPS occultation data in the presence of superrefraction. *J. Atmos. Oceanic Technol.*, **23**, 1629–1644, doi:10.1175/JTECH1996.1.

Yang, D., C. Li, A. K. H. Lau, and Y. Li, 2013: Long-term measurement of daytime atmospheric mixing layer height over Hong Kong. *J. Geophys. Res. Atmos.*, **118**, 2422–2433, doi:10.1002/jgrd.50251.

Zhai, P., and R. E. Eskridge, 1996: Analyses of inhomogeneities in radiosonde temperature and humidity time series. *J. Climate*, **9**, 884–894, doi:10.1175/1520-0442(1996)009<0884:AOIIRT>2.0.CO;2.

Zhang, J., H. Chen, Z. Li, X. Fan, L. Peng, Y. Yu, and M. Cribb, 2010: Analysis of cloud layer structure in Shouxian, China using RS92 radiosonde aided by 95-GHz cloud radar. *J. Geophys. Res.*, **115**, D00K30, doi:10.1029/2010JD014030.

Zhang, Q., J. Zhang, J. Qiao, and S. Wang, 2011: Relationship of atmospheric boundary layer depth with thermodynamic processes at the land surface in arid regions of China. *Sci. China Earth Sci.*, **54**, 1586–1594, doi:10.1007/s11430-011-4207-0.

Zhang, Y., D. J. Seidel, and S. Zhang, 2013: Trends in planetary boundary layer height over Europe. *J. Climate*, **26**, 10 071–10 076, doi:10.1175/JCLI-D-13-00108.1.

Zhao, T., A. Dai, and J. Wang, 2012: Trends in tropospheric humidity from 1970 to 2008 over China from a homogenized radiosonde dataset. *J. Climate*, **25**, 4549–4567, doi:10.1175/JCLI-D-11-00557.1.

Zilitinkevich, S., and A. Baklanov, 2002: Calculation of the height of the stable boundary layer in practical applications. *Bound.-Layer Meteor.*, **105**, 389–409, doi:10.1023/A:1020376832738.